Journal of Extracellular Biology

RESEARCH ARTICLE OPEN ACCESS

Extracellular Vesicle-Associated IL4 Displays Enhanced Anti-Inflammatory Properties in Microglial Cells

Giulia Marostica[1] | Chiara Frigè[1] | Annamaria Finardi[1] | Alessandra Mandelli[1] | Susanna Manenti[1] | Stella Siciliani[1] | Paola Podini[1] | Ivan De Curtis[2,3] | Luca Muzio[1] | Elena Rossi[1] | Paola de Candia[4] | Roberto Furlan[1,2]

[1]Institute of Experimental Neurology, Division of Neuroscience, IRCCS Ospedale San Raffaele, Milan, Italy | [2]Vita e Salute San Raffaele University, Milan, Italy | [3]Cell Adhesion Unit, Division of Neuroscience, IRCCS San Raffaele Scientific Institute, Milan, Italy | [4]Department of Molecular Medicine and Medical Biotechnology, University of Naples Federico II, Naples, Italy

Correspondence: Roberto Furlan (furlan.roberto@hsr.it)

Received: 31 July 2025 | **Revised:** 11 November 2025 | **Accepted:** 6 January 2026

Keywords: anti-inflammatory effect | BV2 | endosomal pathway | extracellular vesicles | interleukin-4 | IL4 receptor | kinetic

ABSTRACT

Neuroinflammation and neurodegeneration are strictly related phenomena, characterized by dysregulation of microglia, central nervous system (CNS) resident immune cells. Interleukin-4 (IL4) has shown beneficial abilities to re-establish microglial homeostasis in experimental models of CNS traumatic injury, stroke and multiple sclerosis, but its optimal administration system remains uncertain. Here, we show that extracellular vesicles (EVs) released by engineered murine microglia BV2 cells constitutively expressing IL4 induced a faster and enhanced anti-inflammatory phenotype in wild type BV2 cells (as assessed by IL4R downstream signalling), compared with soluble IL4. This effect was blunted by an anti-IL4 antibody, while it was not dampened by knocking out the IL4 receptor α subunit in EV-releasing BV2 cells, suggesting that IL4 was localized on the EV surface and did not necessitate to be co-conveyed with the receptor to exert its function. BV2 cells treated with EV-associated IL4, compared with soluble IL4, demonstrated delayed permanence of IL4R in the early endosome, suggesting amplified signalling effects. In conclusion, we here show that the association of IL4 with microglia-derived EVs improve its anti-inflammatory effect in an in vitro murine microglial model, which may inform on novel therapeutic opportunities to restore microglia in human disorders marked by neuroinflammation.

1 | Materials and Methods

1.1 | Cell Culture

Murine microglia cell line BV2 (ICLC ATL03001) was cultured in RPMI 1640 (Gibco) supplemented with 10% FBS (Gibco), L-glutamine (Gibco) 2 mM and penicillin/streptomycin 1% (Gibco) in 5% CO_2 incubator at 37°C.

1.2 | Plasmids

#277-PGK-mIL4 (Figure S1A) and #1514-fGFP (Figure S1B) plasmids were already present in the lab, generated by #277 and #1514 backbones kindly donated by the laboratory of Professor Naldini from our institution. #1514 HRP-TM was generated via cloning. Briefly, pCAG HRP-TM was purchased by Addgene (44441). The plasmid carried BamHI enzymes recognition site,

Giulia Marostica and Chiara Frigè contributed equally to this article.

matched with the optimal cloning site after PGK promoter in #1514-fGFP, realizing with one digestion the excision of fGFP and the creation of suitable cloning sites for the introduction of HRP-TM (Figure S1C). EF1a-Cas9-t2a-PURO plasmid, present in house, was used for the production of IL4Rα-KO BV2 cell line (Figure S1D) in the presence of U-U6-filler-IL4Rsg1-BSD carrying the gRNA targeting the murine IL4Rα subunit (5′-CACCAGCCACTCACACGTGGAAGTG-3′) obtained from Eurofins Genomics (Figure S1E).

1.3 | Lentiviral Production

Lentiviral vectors (277 PGK mIL4, #1514 fGFP, #1514 HRP-TM) were used for the generation of lentivirus. Vectors were produced by transient transfection into human kidney 293T cells. A total of 9×10^6 293T cells were seeded Petri 15 cm^2 for 24 h prior to transfection in Iscove modified Dulbecco culture medium (Sigma–Aldrich, St. Louis, MO) with 10% FBS, 1% P/S and 1% L-G in a 5% CO_2 incubator, and the culture medium was changed 2 h prior to transfection. A total of 59.75 μg of plasmid DNA was used for the transfection of one dish: 9 μg of the envelope plasmid pM (VSV-G), 12.5 μg of packaging plasmid (pMDLg/pRRE), 6.25 μg of REV plasmid, and 32 μg of transfer vector plasmid. The precipitate was formed by adding the plasmids to a final volume of 1125 μL of 0.1× TE/dH_2O (2:1) (1× TE: 10 mM Tris [pH 8.0], 1 mM EDTA) and adding dropwise 125 μL of 2.5 M CaCl2, mixing well and filtering 0.22 μm. Then 1250 μL of 2× HEPES-buffered saline (281 mM NaCl, 100 mM HEPES, 1.5 mM Na2HPO4 [pH 7.12]) were added dropwise while vortexing to the previous solution and immediately added to the cultures. The medium was replaced after 14 to 16 h; the conditioned medium was collected after another 30 h, filtered through a 0.22-μm-pore-size cellulose acetate filter and ultracentrifuged at 65.000 × *g*, 2 h, RT. Viral pellet was resuspended gently in PBS1X and let homogenize at 4°C O/N. Viral particles were aliquoted and stored at −80°C for further use. Viral titre was evaluated by flow cytometry and qPCR.

1.4 | Cell Engineering

To produce engineered BV2 cell lines, BV2 cells were infected at MOI of 10 with the appropriate lentivirus.

Cells were limiting diluted to 1cell/100 μL, plated in MW96 and checked under a microscope for single cell distribution per well. Single cell wells were maintained in culture and passaged to obtain a running stable cell line BV2 IL4 (#277 PGK-mIL4), BV2 fGFP (#1514 fGFP) and BV2 HRP (#1514 HRP-TM), screened by ELISA for BV2 IL4, by flow cytometry and MFI for BV2 fGFP and by a HRP dependent colourimetric assay for BV2 HRP. The selected cell line was expanded and frozen in liquid nitrogen. To generate the KO cell line, BV2 were infected with MOI10 by EF1a-Cas9-t2a-PURO viral particles. After 48 h from the infection, cells were subjected to PURO selection (2.5 μg/mL) for 10 days. Then, cells were infected with MOI10 by lentivirus of guide RNA 1 U6-filler-IL4Rsg1-BSD. Again, after 48 h, cells were limiting diluted to create single-cell-derived lines. After 48 h media was changed for 10 days in selection with BSD. Proliferating single-cell-derived lines were analysed via flow cytometry and western blot analysis for the presence of IL4Rα. The selected single cell line (negative for IL4Rα by both techniques) was expanded and frozen in liquid nitrogen.

1.5 | EVs Isolation and Purification

For EVs isolation, 10^7 BV2 cells were seeded in a 15 cm^2 Petri in RPMI supplemented with 10% EVs depleted-FBS, L-glutamine 2 mM and penicillin/streptomycin 1% and let grow for 48 h at 37 °C in a humidified 5% CO_2 atmosphere. The FBS EV-depleted was produced by an ultracentrifugation (Beckman Optima L-90K Ultracentrifuge) at 100.000 × *g* O/N at 4°C (SW32Ti rotor, Beckman Coulter, Brea, CA) and a subsequent filtration through 0.20 μm filter (Corning). Cells were incubated with 1 μM phorbol 12-myristate 13-acetate (PMA) (Sigma–Aldrich, St. Louis, MO) for 30 min at 37°C. Cell supernatant was collected, and cells and debris were eliminated by centrifugation at 300 × *g* for 10 min at room temperature (RT) and at 2000 × *g* for 20 min at 4°C. Supernatant was filtered through a 5 μm filter (Merck Millipore) and ultracentrifuged at 100.000 × *g* (TH-641 rotor, Thermo Fisher Scientific) for 2 h at 4°C, with consequent elimination of PMA. EVs pellet was resuspended in 1XPBS (Corning) filtered 0.1 μm (Merck Millipore). For Tunable Resistive Pulse Sensing (TRPS), flow cytometry or Transmission Electron Microscopy (TEM) analysis, vesicles were further washed in filtered 1XPBS and ultracentrifuged at 100.000 × *g* for O/N at 4°C and then resuspended in 1XPBS.

1.6 | Fractionation Protocol

Cell supernatant was collected, filtered and centrifuged at 100.000 × *g* for 4 h at 4°C. EVs pellet was resuspended in 1XPBS and centrifuged again at 100.000 × *g* for 4 h at 4°C. The OptiPrep density gradient medium was prepared from 60% stock (Sigma–Aldrich) in ice-cold PBS at the following concentrations: 36%, 30%, 24%, 18% and 12% (Jeppesen et al. 2019). EVs pellet was resuspended in ice-cold PBS, and the iodixanol gradient was layered to decreasing concentration. After a 120.000 × *g* ultracentrifuge for 15 h at 4°C, 12 fractions were collected and distributed in 12 ultracentrifuge tubes. The single fractions were diluted in PBS and again centrifuged at 120.000 × *g* for 4 h at 4°C. Resuspend the pellet in 50 μL of RIPA buffer (NaCl 150 Mm; EDTA 5 mM pH; Tris-HCl 50 mM pH8; NP-40 1.0%; sodium deoxycholate 0.5%; SDS 0.1%) supplemented with protease and phosphatase inhibitors (Sigma–Aldrich). Total protein level was quantified through Micro BCA Protein Assay Kit (Thermo Fisher Scientific), and samples were stored at −80°C.

1.7 | Tunable Resistive Pulse Sensing (TRPS)

Size distribution, concentration and ζ (zeta) potential of isolated EVs were measured by qNano instrument (Izon Science Ltd.), based on TRPS technology. The instrument was set according to the manufacturer's instructions for the measurement. NP150 nanopores (Izon Science) and calibration particle CPC100 beads (Izon Science) were used. Samples were diluted in measurement electrolyte (0.1 μm filtered PBS + 0.3% wetting solution, Izon Science) to achieve a particle flow between 200 and 400 particles per minute. Pore stretch, voltage and pressure were maintained

TABLE 1 | EVs donor cell lines list.

Cell line denomination	Engineering/treatment	Phenotype
NS BV2	Non stimulated BV2	—
rIL4 BV2	BV2 treated for 12 h with 10 ng/mL rIL4	—
Eng IL4 BV2	BV2 infected with #277 PGK-mIL4 lentiviral vector, clone#47	BV2 expressing constitutively IL4
Eng fGFP BV2	BV2 infected with #1514 fGFP lentiviral vector	BV2 expressing constitutively farnesylated C-terminal GFP on cell membranes
Eng HRP BV2	BV2 infected with #1514 HRP-TM lentiviral vector	BV2 expressing constitutively HRP associated to the transmembrane domain of the PDGFRβ on cell membranes
Eng HRP IL4 BV2	BV2 infected with #1514 HRP-TM and #277 PGK mIL4 lentiviral vector	BV2 expressing constitutively HRP on cell membranes and IL4
IL4Rα-KO BV2	BV2 infected with EF1a-Cas9-t2a-PURO and U6-filler-IL4Rsg1-BSD lentiviral vectors	BV2 CRISPR Cas9 depleted of IL4Rα
Eng IL4 IL4Rα-KO BV2	CRISPR Cas9 for IL4Rα and infected with #277 PGK mIL4 lentiviral vector	BV2 depleted of IL4Rα and expressing constitutively IL4

constant between samples and calibration while measuring size and concentration. Instead, while measuring ζ potential, pressure, and voltage could be modulated in the range of calibration. Samples were analysed until 500 particles were counted. Data processing and analysis were done on the Izon Control Suite software v3.4. The Gauss distribution was matched to histograms.

1.8 | BV2 phenotype Induction

BV2 cells were subjected to mouse recombinant IL4 (rIL4) (R&D system) 10 ng/mL for 12 h, recombinant IFNγ (rIFNγ) (Preprotech) 20 ng/mL for 12 h or for 8 h with EVs, isolated from NS BV2, rIL4 treated BV2 or Eng IL4 BV2. The proportion between administered EVs and recipient cells was 1000 to 1. The information about donor cells and relative EVs are described in Tables 1 and 2, respectively. Cells were then collected, lysed in TRIzol Reagent (Invitrogen) and stored at −80°C. The expression of anti-inflammatory markers, Arg1 and Ym1, and of pro-inflammatory ones, IL1beta and INOS, were evaluated.

1.9 | rIL4 Dose-Response Curve and EVs Dose-Response Curve

For the rIL4 dose-response curve, 2×10^5 BV2 cells were seeded in MW24 and after 24 h treated with different concentration of rIL4 for 12 h. The EVs dose-response curve was instead obtained by treating a constant number of 2×10^5 BV2 cells 8 h with an increasing number of EVs obtained from NS BV2 or Eng IL4 BV2. Cells are lysed with TRIzol Reagent and stored at −80°C. The expression of anti-inflammatory marker Arg1 was evaluated.

1.10 | Recombinant IL4 Neutralization Assay

For neutralization assay, rIL4 (10 ng/mL) and different concentration of neutralizing IL4 antibody (R&D system) were incubated in medium for 1 h at 37°C in 5% CO_2 incubator. The medium was then used to treat for 12 h, previously seeded 2×10^5 BV2 cells in a MW24. Cells were lysed with TRIzol Reagent and stored at −80°C. The expression of anti-inflammatory marker Arg1 was evaluated.

1.11 | Kinetic Studies

2×10^5 BV2 were seeded in MW24 and after 24 h treated for different time intervals (0, 1, 3, 6 or 8 h) with 2×10^8 vesicles/well or rIL4 (10 ng/mL). The different donor cell lines and the corresponding EVs exploited as treatment are described in Tables 1 and 2, respectively. Cells were lysed with TRIzol Reagent and stored at −80°C. The expression of anti-inflammatory markers Arg1 and Ym1 were evaluated.

1.12 | Extracellular Vesicles Uptake Studies

2×10^5 BV2 cells were seeded in MW24 and after 24 h pre-treated with 50 μM chloroquine diphosphate salt (CQ) (Sigma–Aldrich) for 2 h. Cells were washed with 1XPBS for two times and then incubated with fGFP fluorescent vesicle for different time periods. The proportion between administered EVs and recipient cells was 1000 to 1. At the end of the treatment, cells were washed two times with ice-cold PBS and detached using trypsin-EDTA 0.25% (Gibco) for 10 min at 37°C in 5% CO_2 incubator. Detached cells were collected and processed according to the flow cytometry protocol.

TABLE 2 | EVs list.

EV denomination	EV pre-treatments
EVs from NS BV2	—
EVs from rIL4 BV2	—
EVs from Eng IL4 BV2	—
EVs from Eng IL4 BV2 + IgG	Incubated for 1 h at 37°C with isotype control Rat IgG1
EVs from Eng IL4 BV2 + αIL4	Incubated for 1 h at 37°C with neutralizing IL4 antibody
IL4 decorated EVs	EVs from NS BV2 incubated with rIL4 10 ng/mL
EVs from IL4Rα-KO BV2	—
EVs from rIL4 IL4Rα-KO BV2	—
EVs from Eng IL4 IL4Rα-KO BV2 + IgG	Incubated for 1 h at 37°C with isotype control Rat IgG1
EVs from Eng IL4 IL4Rα-KO BV2 + αIL4	Incubated for 1 h at 37°C with neutralizing IL4 antibody
EVs from Eng fGFP BV2	—
EVs from Eng HRP BV2	—
EVs from Eng HRP IL4 BV2	—

1.13 | RNA Extraction and Retrotranscription

RNA extraction was performed on cell lysed with TRIzol Reagent according to the manufacturer's protocol. Dissolved RNA was then treated with RQ1 RNase-Free DNase (Promega) for the digestion of contaminating genomic DNA. The resulting purified RNA was mixed again with TRIzol Reagent and isolated according to manufacturer's protocol.

RNA extraction from vesicles was carried out using NucleoSpin miRNA (Macherey-Nagel) according to manufacturer's protocol.

RNA retrotranscription was performed using High-Capacity cDNA Reverse Transcription Kit (Applied Biosystems). An RT negative control lacking the reverse transcriptase was always inserted in the retrotranscription, to assess possible contamination of genomic DNA.

1.14 | Quantitative Real-Time PCR Analysis

Two different analysis methods (Taqman probe and SYBRGreen probe) were used depending on the number of samples. For SYBRGreen qPCR, iTaq Universal SYBR Green Supermix (Biorad) was mixed with in-house designed forward and reverse primer (Table S1) at final concentration of 10 μM and added to cDNA for probing. For Taqman qPCR, TaqmanTM Fast Advanced Master Mix (Applied Biosystem) was mixed with Taqman gene probe (Table S2).

The following program was used to perform qRT-PCR: 10 ng of cDNA as template, 1 μL (10 pmol. μL^{-1}) of each primer, 10 μL SYBR Green SuperMix 2X in a total volume of 20 μL. qRT-PCR was run at 95°C (180 s), 40 cycles at 95°C (5 s), 65°C (30 s), followed by melting curve from 95°C (15 s) to 60°C (60 s), and a dissociation step at 95°C (15 s). Cycle thresholds (C(t)s) were analysed using Livak method ($2^{-\Delta\Delta Ct}$), and relative expression levels were calculated using the Microsoft Excel software.

1.15 | Elisa

DuoSet ELISA kits (R&D System) were used to quantify murine IL4 levels in EVs from NS BV2, rIL4 treated BV2 or Eng IL4 BV2, according to manufacturer's protocol.

1.16 | Flow Cytometry

Megamix-Plus FSC (BioCytex) were used to set physical gates for EVs and similar events. EVs were stained 1:100 with Isolectin GS-IB_4 from Griffonia simplicifolia Alexa Fluor 647 Conjugate (Thermo Fisher Scientific) or with 1:100 IB_4 blocked by melibiose (IB4 was pre-incubated 1:10 with melibiose 0.1 M for 30 min 4°C) (Sigma–Aldrich, St. Louis, MO) for 30 min 4°C. EVs were diluted 1:200 final in 1XPBS before analysis with CytoflexS Flow Cytometer. For EVs uptake experiment, cells were stained intracellularly according with the protocol of BD Cytofix/CytopermTM Plus (BD Biosciences), using Fc block (1:50) (BioLegend) to avoid aspecific binding, anti-GFP (1:50) and its corresponding isotype.

1.17 | Immunofluorescence

BV2 cells were seeded on poly-D-lysine (Sigma–Aldrich) and laminin (Sigma–Aldrich) coated slides for 48 h to allow proper adhesion. Cells were treated and washed in PBS twice, then fixed in paraformaldehyde 4% (Sigma–Aldrich) for 15 min RT, washed three times with 1XPBS, and incubated with glycine (Sigma–Aldrich) 0.1 M per 10 min RT. Cells were washed in PBS 3 times, blocked in blocking solution with or without detergent (10% serum; 0.1% Triton-X; 1XPBS) for 1 h at RT. Primary antibodies were diluted in 1% serum blocking solution and incubated O/N at 4°C. The following day, cells were washed three times in 1XPBS and probed with the suitable secondary antibody diluted in 5% serum blocking solution, for 2 h at RT. Then, cells were washed three times in 1XPBS for 5 min and incubated in DAPI (1:25.000) (Roche Diagnostics Spa, Monza, Italy) for 1 min for nuclei counterstaining. At the end, circular glasses were mounted in a super

frost glass using fluorescent mounting medium (Dako North America). Surface stain was performed with Iba1 (1:200) (NB100-1028, NovusBio) or CD11b (1:100) (MCA74GA, Biorad), and intracellular stain was performed with GFP (1:500) (Millipore), Rab5 (1:200) (NovusBio), Rab7 (1:200) (NovusBio) and lamp1 (1:500) (NovusBio) and IL4Ra (Santa Cruz). Secondary antibodies were DkαGT633 (Thermo Fisher Scientific), GtαCK488 (Thermo Fisher Scientific) and GtαRb546 (Thermo Fisher Scientific). Leica TCS SP8 SMD FLIM Laser Scanning Confocal microscope was used to acquire slide images. Each experimental condition was performed in duplicate and five images were acquired for each slide. Fluorescence and colocalization analysis were done using ImageJ software and ARIVIS software.

1.18 | Protein Quantification

Cells and EVs were lysed in home-made 1XRipa lysis buffer or in 1XTEN solution with protease and phosphatase inhibitor cocktail (Sigma–Aldrich), via mechanical homogenization. Cells and EVs protein quantity was measured using a Pierce BCA Protein Assay Kit (Thermo Fisher Scientific) and a Micro BCA Protein Assay Kit (Thermo Fisher Scientific), respectively, according to manufacturer's protocol. Proteins were stored at −80°C.

1.19 | Western Blot and Ab probing

Quantified proteins were aliquoted and boiled with Laemmli buffer (4% sodium dodecyl sulfate (SDS), 20% glycerol, 0.1 mM Tris pH 6.8, and 0.005% of bromophenol blue) for 5 min at 100°C. Samples were resolved in SDS-PAGE gels (12% handmade gels or 4%–20% Mini-PROTEAN TGX Precast Protein Gels, Biorad), and gels were blotted onto 0.45 μM nitrocellulose membranes (Amersham) via Trans-Blot Turbo Transfer System (Biorad). Membranes were blocked for nonspecific sites with 5% non-fat dry milk in 1XTBS-Tween20 (TBS-T) (50 mM Tris-HCl, 150 mM NaCl, pH 7.5, 0.1% Tween20) for 1 h at RT, then membranes were incubated with primary antibodies (Table S3), diluted in blocking solution, O/N at 4 °C. Next, membranes were washed with TBS-T (3 × 10 min) and incubated with secondary antibody at RT for 2 h. Secondary antibodies used were: goat anti-mouse IgG HRP (Biorad) and goat anti-rabbit IgG HRP (Biorad). After washing, Clarity ECL Western Blotting Substrates (Biorad) were used to visualize bands at ChemiDoc Touch (Biorad).

1.20 | Electron Microscopy for Immunogold Labelling

$8*10^6$ cells were seeded in a 10 cm^2 Petri dish and treated according to the experiment design. Cells were detached with trypsin-EDTA and centrifuged for 10 min at 300 × *g*. Cells were fixed in 4% PFA + 0.1% glutaraldehyde for 2 h at 4°C. Cells were washed three times in PBS and stored at 4°C. The cell pellet was included in 2% low-gelling temperature (Sigma–Aldrich) using frozen support. Cell pellet is stored temporarily in MilliQ H_2O and dehydrated in graded ethanol of 30%, 50%, 70% twice each time for 10 min, in 90% ethanol for two times 15 min and finally in 100% ethanol for three times 10 min. Sample was left for 30 min at 4°C in activated LR-white, LR-white was substituted, and samples were left O/N at 4°C in solution. The next day, samples were placed in new LR-white and left in oven at 60°C O/N. Solidified samples were cut and placed on grids. Grids were prepared for immunogold staining. Briefly, grids were blocked in 1:50 normal goat serum (NGS) for 3 min at RT and probed with IL4 (1:150) (Santa Cruz Biotechnologies) and IL4R (1:150) (BIOSS antibody) antibodies at 4°C O/N in a humidified chamber. The day after, grids were washed twice in PBS-0.1% Tween for 5 min, twice in PBS for 5 min, blocked in 1:50 NGS for 5 min at RT and probed for 30 min at RT with secondary antibodies anti-goat (EM rabbit anti-goat IgG immunogold conjugate 15 nm, EM.RAG15, BBI solutions) and anti-rabbit (EM goat anti-rabbit IgG immunogold conjugate 5 nm, EM.GAR5, BBI solutions). Then grids were washed twice in PBS for 5 min and twice in MilliQ H_2O for 5 min. Finally, grids were stained for 2 min with uranyl acetate (Honeywell Fluka), washed with MilliQ H_2O, and stained with lead citrate (Sigma–Aldrich). Samples were analysed via TEM FEI Talos L120C G2 Transmission Electron Microscope.

2 | Introduction

Clinical and mechanistic studies concur to demonstrate that most neurological diseases are fuelled by a dysregulated immunological component, known as neuroinflammation, which is mediated by reactive oxygen species, pro-inflammatory cytokines and secondary messengers, and involves both resident and peripheral immune cells in the central nervous system (CNS) (DiSabato et al. 2016). Beside multiple sclerosis (MS), a prototypic disease caused by an autoimmune response toward the CNS, several other neurodegenerative diseases, including Alzheimer disease (AD) and Parkinson's disease (PD), although not canonically inflammatory, are characterized by an aberrant activation of CNS-resident macrophages, microglia, believed not to simply drive the progression of neuronal damage but to actively contribute to its initiation (Gao et al. 2023; Ransohoff 2016; Yong 2022; Zhang et al. 2023).

Microglia is fundamental for the correct brain development, and it keeps supporting the health of the adult brain by constantly scanning the surrounding environment and dynamically changing its morphology and activity in response to environmental stimuli (Chen and Trapp 2016; Li and Barres 2018; Prinz et al. 2019).

Microglial cells can be experimentally polarized toward the so-called 'canonical' activated M1 pro-inflammatory and 'alternative' activated M2 anti-inflammatory phenotype, following exposure to well-known pro or anti-inflammatory stimuli, such as Interferon γ (IFN γ) and LPS or Interleukin 4 (IL4), respectively (Orihuela et al. 2016).

IL4, mainly secreted by TH2-like cells, but also by granulocytes and myeloid cell (Egholm et al. 2019), has demonstrated a key immunoregulatory role in healthy CNS (Derecki et al. 2010; Gadani et al. 2012; Guedes et al. 2023; Quarta et al. 2020). Consistently, in recent decennia, IL4 has emerged as a neuroprotective, regeneration-inducing agent in experimental models of CNS traumatic injury, stroke and MS (Gärtner et al. 2023; Jiang et al. 2022; Wang et al. 2024). In particular, the intrathecal injection of IL4 carried by viral vectors has been shown to have a protective

and well-tolerated effect against the pathological progression of Experimental Autoimmune Encephalomyelitis (EAE), a model of MS, in mice and Rhesus Monkeys (Butti et al. 2008; Casella et al. 2016; Furlan et al. 2001; Poliani et al. 2001). Nonetheless, the identification of either artificial or biological carriers able to potentiate the effect and/or the specificity of IL4 administration is still elusive.

A highly promising group of potential cytokine carriers is represented by extracellular vesicles (EVs), nanometric membrane-delimited particles released by virtually all cells, and relevant actors of cell-to-cell communication (Buzas 2023; Welsh et al. 2024; Yáñez-Mó et al. 2015). In CNS, released by both neurons and glial cells, EVs have demonstrated important immunomodulatory abilities and play roles in both homeostasis or pathogenic state (Delpech et al. 2019; Hermann et al. 2023; Lizarraga-Valderrama and Sheridan 2021). In particular, the composition of EVs released by microglia reflects the dynamic nature of this cell population and represents a specific signature of its activation state: microglia-derived EVs were shown to modulate multiple processes in the CNS, such as synaptic activity in neuronal cells, myelination in oligodendrocyte precursor cells (OPC), astrocyte phenotype, neo-angiogenesis and the function of other microglial cells (Gabrielli et al. 2022). EVs are able to cross the BBB in both directions, acting as a link between the CNS and the periphery. This transition is largely boosted in pathological processes, such as neurodegeneration, brain injury and inflammation. Consequently, EVs can be considered a potential window to peek into the health state of the CNS and a drug delivery tool (Agliardi and Clerici 2020; Krämer-Albers 2022; Mustapic et al. 2017; Saint-Pol et al. 2020; Wiklander et al. 2019). Concerning this last point, we observed that intrathecal injection of EVs associated IL4, with tropism towards CNS phagocytic cells, were able to modulate neuroinflammation and clinical symptoms and neuropathological features in EAE mouse model (Casella et al. 2018).

With the aim of exploring the potential of EVs as a profitable strategy to reduce microglia-dependent neuroinflammation, we have here decided to investigate whether the delivery of IL4 through microglia-derived EVs may enhance its natural anti-inflammatory polarizing efficiency, utilizing a flexible murine microglia in vitro system.

3 | Results

3.1 | Engineering of Murine Microglia for the Production of IL4-Enriched Extracellular Vesicles

We first engineered murine neonatal immortalized BV2 microglial cells, commonly used to study microglial phenotype and function (Blasi et al. 1990; Quarta et al. 2020), with a #277 PGK-mIL4 lentiviral vector to constitutively express IL4 (Eng IL4 BV2); alternatively, we treated the same cells with recombinant IL4 (rIL4 BV2) or left them not stimulated at all (NS BV2) (experimental scheme in Figure 1A). We then isolated the EVs released by these three cell populations (Eng IL4 BV2, rIL4 BV2 and NS BV2) from the supernatant by differential centrifugation (upon 48 h of cell culture) and quantified for their IL4 content, finding that, relative to the total protein cargo, EVs derived from Eng IL4 BV2 cells contained a significantly higher quantity of IL4, compared to those released by either rIL4 BV2 and NS BV2 cells (Figure 1B). By exploiting TRPS, we assessed that the number, size distribution, and physical properties of BV2-derived EVs were not appreciably modified by either rIL4 stimulation or IL4 engineering (Figure 1C,D).

Next, we utilized an Iodixanol density gradient to analyse the composition of the EVs pellet derived by the ultracentrifugation of Eng IL4 BV2 medium. We assessed the enrichment of vesicular markers (i.e., ALIX and FLOTILLIN-1) in fractions 3-to-6 and that of non-vesicular markers (GAPDH and HISTONE 3, H3) in fractions 6-to-10 (Figure 1E). IL4 quantification by ELISA on the Iodixanol density gradient fractions, relative to the total protein content, revealed that IL4 was present in detectable amount in most of the fractions (Figure 1F). Further, TRPS analysis confirmed the EV localization mainly in the 1 to 6 fractions, called 'Vesicular fractions' (Figure 1G). Additional quantification of IL4 by ELISA in all fractions revealed higher levels of IL4 in the vesicular fractions, (222.01 pg/mL), compared with lower levels in the non-vesicular fractions (46.64 pg/mL). The parallel evaluation of the EV number by TRPS with the IL4 quantity by ELISA led to assess that 2×10^8 EVs released by Eng IL4 BV2 cells, the amount used for in vitro studies, shuttled around 0.58 pg of IL4, while the non-vesicular fractions contained around 0.06 pg of IL4 (Figure 1G,H).

In summary, we engineered BV2 cells to overexpress IL4 for the production of EVs with quantitative and qualitative properties comparable to those released by parental BV2 cells, but with substantially increased IL4 cargo.

We then tested the anti-inflammatory properties of those EVs, in comparison with the soluble form of rIL4.

3.2 | EVs From Eng IL4 BV2 Display a Stronger and Faster Anti-Inflammatory Effect Than Soluble rIL4

In order to monitor the IL4-dependent induction of a 'M2-like microglia' phenotype in BV2 cells, we treated the cells with EVs released by Eng IL4 BV2 cells. First, to directly compare rIL4 and Eng IL4 BV2-derived EVs in terms of the efficacy of their M2 polarization activity on BV2 cells, we performed a dose-response assay on Arg1 expression. While BV2 cells responded to rIL4 at the dose of 1 ng/mL and reached a plateau at 10 ng/mL, the same cells responded to Eng IL4 BV2-derived EVs (but not to NS BV2-derived EVs) at the dose of 2×10^8 EVs/2×10^5 cells corresponding to 1000 EVs/cell (Figure 2A,B). To further confirm the obtained results, treated cells were analysed for the expression of both Arg1 and Ym1, finding that EVs were able to induce the expression of both Arg1 and Ym1 in comparison with the treatment with rIL4 (Figure S2A,B). When BV2 cells were pre-treated with IFNγ, mimicking an inflammatory condition, EVs from Eng IL4 BV2 were capable to induce high levels of Arg1 and Ym1 expression (Figure S2C,D), and they also hampered the activation of the key pro-inflammatory mediator IL1β (although not that of iNOS, Figure S2E,F).

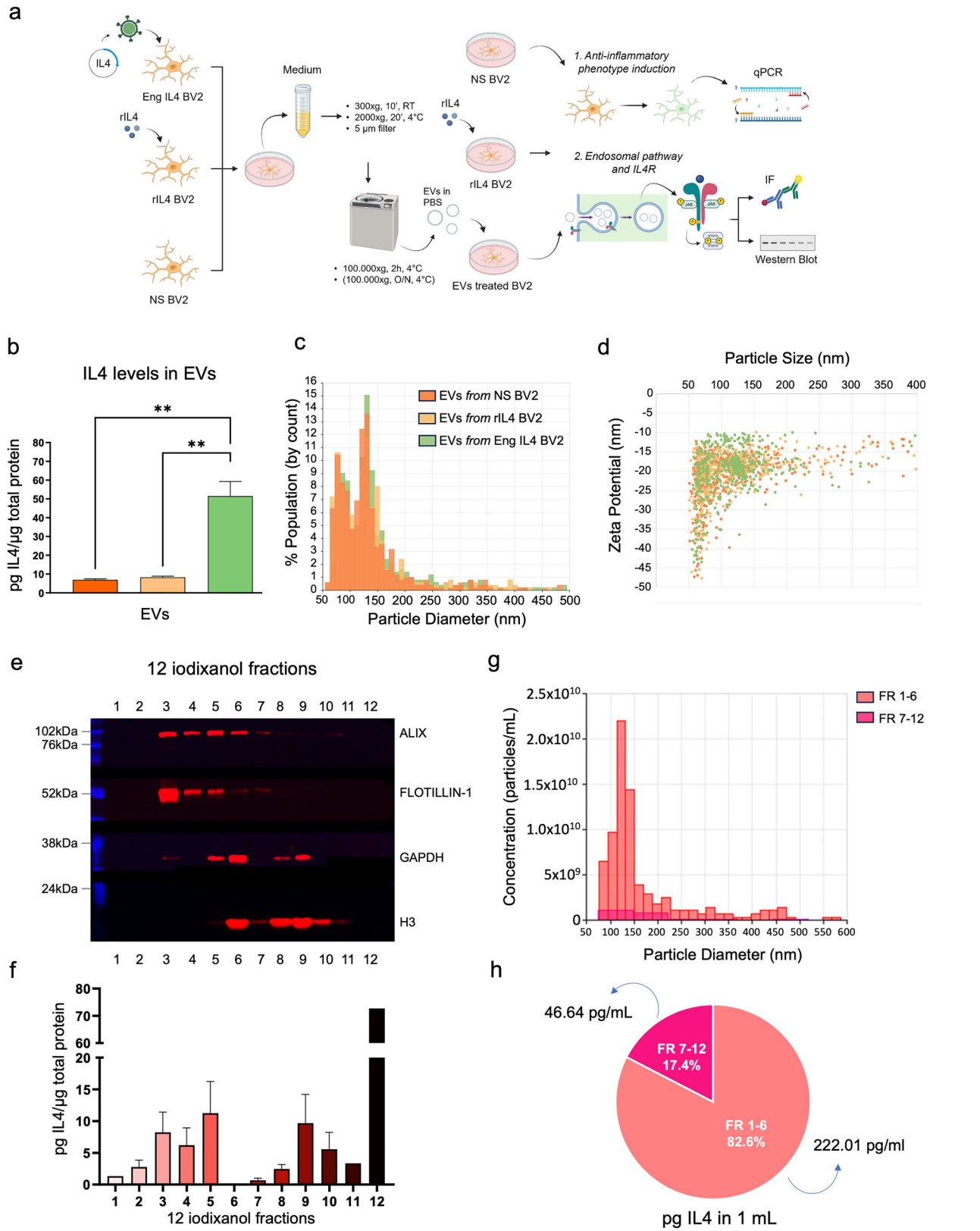

FIGURE 1 | Characterization of Engineered BV2 IL4-enriched extracellular vesicles. (a) Simplified scheme of the project. Made with BioRender. (b) Elisa IL4 content in ultracentrifuged isolated EVs from not stimulated (EVs *from* NS *BV2*; Orange), rIL4 treated (EVs *from* rIL4 BV2; Light orange), and IL4 engineered BV2 (EVs *from* Eng IL4 BV2; Green). Data are the mean of three independent replicates for each condition. Data are shown as mean ratio between IL4 quantity in pg measured with ELISA kit and whole protein content in µg measured with BCA assay (mean ± SEM). Ordinary one-way ANOVA, corrected with Tukey's multiple comparisons test. (c–d) Size and superficial charge Evs characterization by Tunable Resistive Pulse Sensing (TRPS), qNano; The graphs show (c) particle diameter on x-axis with concentration (particles/mL) on y-axis, and (d) particle diameter on x-axis with zeta potential (mV) on y-axis, of EVs *from* NS *BV2* (Orange), EVs *from* rIL4 BV2 (Light orange) and EVs *from* Eng IL4 BV2 (Green). (e) Western blot

We thus experimentally identified that the minimum ratio EVs/cell necessary to induce a detectable polarization, *was* 1000 EVs/cell (Figure 2B).

We next analysed the anti-inflammatory gene expression kinetics, by quantifying both Arg1 and Ym1 at different time points upon treatment start (0, 1, 3, 6, 8 h) with either rIL4 at a concentration of 10 ng/mL (3 ng/2 × 10^5 cells) or Eng IL4 BV2-derived EVs (2 × 10^8 EVs/2 × 10^5 cells), corresponding to 0.58 pg of EV-associated IL4 (less than 1 pg total including also the non-vesicular fractions). Surprisingly, whilst rIL4 was used at a concentration 5.000 times higher than that shuttled by EVs, we found that both Arg1 and Ym1 were induced more rapidly and at higher levels in cells treated with Eng IL4 BV2-derived EVs compared with soluble rIL4 (Figure 2C,D).

Intriguingly, the registered anti-inflammatory effect of IL4 (in terms of Arg1 and Ym1 expression) could be dramatically impaired by an IL4 neutralizing antibody (αIL4) (Figure S2G) used in pre-incubation with Eng IL4 BV2-derived EVs prior to treatment with recipient cells, suggesting a localization of IL4 on the surface, or at least outside of EVs (Figure 2C,D). To directly test whether a mere localization of IL4 outside EVs may retain its enhanced anti-inflammatory activity, we produced 'rIL4 decorated' EVs by incubation of EVs from NS BV2 cells with rIL4 at the same concentration used for the rIL4 treatment. When administered to recipient BV2 cells, the 'rIL4 decorated' EVs indeed promoted an anti-inflammatory phenotype shift comparable to that induced by Eng IL4 BV2-derived EVs, confirming that EVs are able to augment IL4 activity (Figure 2E,F).

Since it is known that EVs can transport cytokines as well as their respective receptors (Buzas 2023), we decided to evaluate the contribution of IL4 receptor (IL4R) to the biological function of EVs from Eng IL4 BV2.

To this aim, we produced a BV2 cell line with a specific IL4Rα gene knockout (IL4Rα-KO BV2) by CRISPR-Cas9 gene editing, eliminating the IL4Rα subunit (Figure S2H) involved in both type I and II IL4 signalling pathway (Bernstein et al. 2023; Junttila 2018). Subsequently, IL4Rα-KO BV2 cell line was engineered with #277-PGK-mIL4 lentiviral vector for the over-expression of IL4. The EVs released by these Eng IL4 IL4Rα-KO BV2 cells, which cannot co-shuttle IL4R with IL4, resulted to retain the capability to induce both Arg1 and Ym1 expression in BV2 target cells, demonstrating that EV-associated IL4R is not involved in the IL4 biological effect observed (Figure 2G,H).

In summary, IL4 in association with EVs (released by Eng IL4 BV2 cells) was found to be dramatically more efficacious in its capacity to induce an anti-inflammatory phenotype in BV2 cells. We then decided to investigate whether this higher anti-inflammatory effect may depend on different internalization kinetics of IL4R in the case of EV-associated IL4, compared with rIL4.

3.3 | Delayed IL4R Translocation Across the BV2 Cell Endosomal Pathway Upon EV-Associated IL4 Treatment

One of the most accredited mechanisms involved in EV cell-to-cell communication is through endocytosis (Mulcahy et al. 2014). To test whether this was indeed the mechanism by which EVs were up-taken by BV2 cells, we started by creating an engineered BV2 cell line expressing a GFP protein modified with a farnesylated C-terminal (fGFP), that guaranteed GFP anchoring to cell membrane (Eng fGFP BV2 cells). These cells were able to release EVs marked by fGFP protein, that could be followed in the recipient cells. The presence of fGFP marker was assessed by western blotting and FACS analysis, in comparison with EVs from NS BV2 cell line (Figure S3A–C). Those EVs also contained the expected microglia marker IB4, and serial dilution confirmed the direct association between the number of IB4+ and fGFP+ particles (Figure S3D). We then perturbed the endosomal pathway physiology by using the chloroquine diphosphate salt (CQ), an inhibitor of lysosome acidification, and we treated BV2 cells with EVs from Eng fGFP BV2 cells, showing that both the percentage of $fGFP^+$ BV2 cells and the quantity of fGFP present in late endosome significantly increased in cells pretreated with CQ, which suggested a prominent endosomal-dependent up-take of those EVs (Figure S3E,F). We also followed the fate of EV-associated fGFP in EV target cells by immunofluorescence experiment, investigating the colocalization with typical endosomal pathway compartment markers, Rab5, Rab7 and Lamp1 (early endosome, late endosome and lysosome markers, respectively). We observed that EV-associated fGFP peaked in early endosomes 1 h after EV treatment and then culminated in late endosomes 2 h later (Figure 3A,B).

Since the IL4 signalling seems to require IL4R subunits internalization (Gandhi et al. 2014a), we decided to explore the localization of IL4Rα subunit across the endosomal pathway. To this aim, we exploited, first of all, a BV2 cell line expressing a membrane-bound HRP (electron dense in electron microscopy) and engineered it with #277 PGK mIL4 lentiviral vector in order to isolate EVs decorated with HRP and IL4-enriched (EVs from Eng HRP IL4 BV2). Double immunogold studies targeting IL4Rα and IL4 on BV2 cells, incubated with EVs from Eng HRP IL4 BV2, confirmed the presence of IL4Rα at the level of the endosomal compartment (Figure 3C).

Then we analysed the kinetics of IL4Rα internalization by its immunofluorescence colocalization with the endosomal/lysosomal markers (i.e., Rab5, Rab7 and Lamp1),

assay on 12 iodixanol fraction to assess vesicular, ALIX (105 kDa) and FLOTILLIN-1 (47 kDa), and non-vesicular markers, HISTONE 3 (H3) (17 kDa) and GAPDH (37 kDa). (f) Elisa IL4 quantification in 12 iodixanol fraction normalized for total protein content via BCA assay. Data are shown as mean ratio between IL4 quantity in pg measured and whole protein content in μg (mean ± SEM). (g) TRPS measurement of EVs present in the vesicular (FR 1-6) and non-vesicular fraction (FR 7-12) after iodixanol isolation. Size distribution, with particle diameter on x-axis and concentration (particles/mL) on y-axis. Vesicular fraction is depicted in light pink, non-vesicular fraction in dark pink. (h) Percentage of Elisa IL4 content in pg in 1 mL of vesicular (1-6), 82.6%, and non-vesicular fraction (7-12), 17.4%. Significance is expressed as follows *$p < 0.05$; **$p < 0.01$; ***$p < 0.001$; ****$p < 0.0001$.

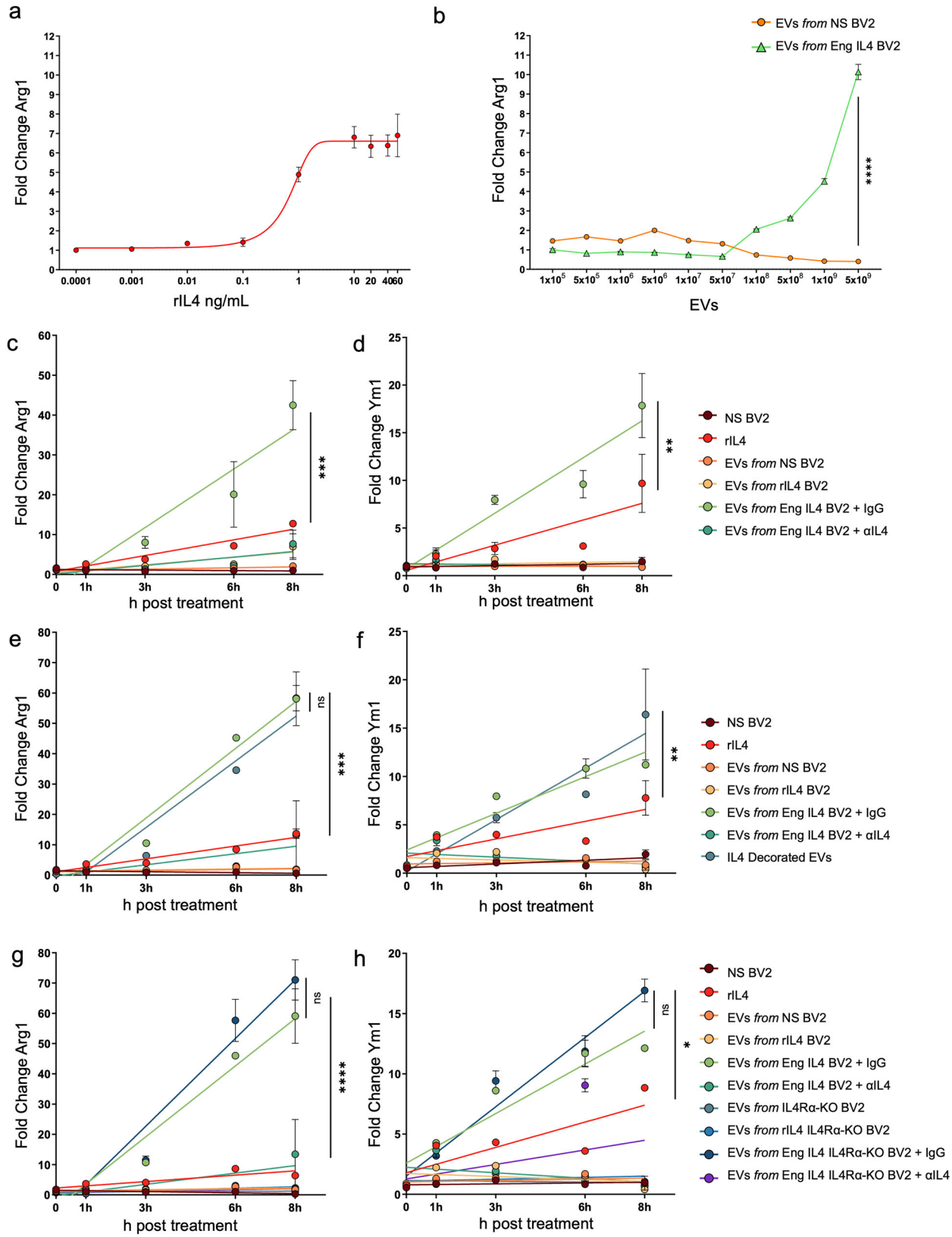

FIGURE 2 | Comparison between soluble rIL4 and EVs delivering IL4 in terms of anti-inflammatory phenotype induction. (a) rIL4 dose response curve and (b) EVs *from* NS BV2 (Orange) or EVs *from* Eng IL4 BV2 (Green) dose response curve. Evaluation of anti-inflammatory markers Arg1 expression by real-time PCR. Gapdh was used as housekeeping gene and data are shown as fold change increment of Arg1 mRNA on NS BV2 (FC ± SEM). In EVs

in BV2 cells treated with either rIL4 or EVs from Eng IL4 BV2 cells at different time points (0, 15', 30', 1, 2 and 3 h) after the treatment (Figure 3D). We observed that, while in BV2 treated with rIL4 the majority of IL4Rα spread from early into late endosomes between 15 and 30 min, after EV treatment IL4Rα lingered in the early endosome for more time, being still high at 30 min (Figure 3E,F). Furthermore, IL4Rα colocalized with lysosomes 2 h after treatment only with rIL4 alone (Figure 3G). The difference in the kinetic of IL4Rα localization across the endosomal pathway actually suggests that a delayed passage from early into late endosome compartment and then into lysosomes in the case of IL4 associated to EVs, compared with rIL4 alone, could help IL4 signalling and, in particular, the IL4 endosomal signalling.

3.4 | Higher STAT6 Phosphorylation in BV2 Cells Upon EV-Associated IL4 Treatment

It is recognized that one of the main molecular pathways downstream of IL4 signalling is the JAK-STAT pathway, which activation results in the phosphorylation of STAT6 (P-STAT6) and its homodimerization (Bernstein et al. 2023). In particular, the M2 polarization shift of microglia/macrophages was shown to be mediated by JAK1/STAT6 after IL4 treatment (He et al. 2020). By western blot analysis, we found that the quantity of P-STAT6 in BV2 cells treated with Eng IL4 BV2-derived EVs was significantly higher 30 min after treatment initiation, compared to rIL4-treated cells, suggesting that the higher polarizing capacity of EV-associated IL4 was indeed linked to an enhanced intracellular signalling of the relevant downstream phosphorylation events (Figure 3H).

4 | Discussion

Nowadays, the development of neuroprotective/neurodegenerative treatments able to prevent or repair axon damage in neurodegenerative conditions is a medical need of utmost importance. In this regard, IL4-based therapeutic strategies have the potential to benefit several human disorders of the CNS, including traumatic injury, stroke and neuroinflammation (Gärtner et al. 2023). The specific delivery of IL4 into the CNS is a fundamental prerequisite, which would allow to circumvent the short half-life and potential side effects of systemically administered cytokines (Deckers et al. 2023; Saxton et al. 2023), as well as the obstacle of the Blood Brain Barrier (BBB) (Erickson and Banks 2018). Intrathecal direct administration of IL4 or viral vectors encoding for IL4 gene ameliorate clinical score and promote neuroprotection in EAE murine model of MS (Butti et al. 2008; Furlan et al. 2001, Furlan et al. 1998; Vogelaar et al. 2018) and in Rhesus Monkeys affected by a hyper-acute form of EAE (Poliani et al. 2001). Nonetheless, the capability to reach the CNS by systemic administration remains unmet. EVs are indeed capable of delivering a specific cargo (an siRNA) into the brain when injected systemically, and to efficiently knock down the expression of the target gene in neurons, microglia, and oligodendrocytes in the brain (Alvarez-Erviti et al. 2011). Besides the advantage of crossing the BBB, EVs are also believed to display low immunogenicity and, differently from both viral vectors and lipid nanoparticles, they may shuttle a plethora of molecules, other than the specific cargo, with potential synergistic anti-inflammatory effect. Now, while we have previously reported that EVs of murine microglial origin, injected in the cisterna magna of EAE mice, are able to deliver IL4 and to curb the ongoing neuroinflammatory disease (Casella et al. 2018), the present work adds on that study by demonstrating that the use of microglial EV-associated IL4 may actually have a substantial and objective therapeutic advantage in terms of the capacity to elicit the desired anti-inflammatory response in target microglia.

We used BV2 cells, a murine microglia cell line (Blasi et al. 1990), as the source of isolated EVs, since it has already been described that microglia-derived EVs are preferentially taken up by other microglia cells (Verderio et al. 2012). Moreover, we used a composite population of isolated EVs (containing both exosomes and larger particles) as this heterogeneity has been previously demonstrated to increase the cell-to-cell communication capability (Kanada et al. 2015).

The most relevant result of the present work is that, when delivered in association with EVs, IL4 was able to induce the M2 transcriptional signature in microglial cells at significantly lower concentration and sensibly faster than what registered for the soluble form of the cytokine.

Our cell biology experiments suggest that the ability of EVs to more efficiently activate IL4-dependent signal transduction may rely on the different kinetics in IL4R localization across the endosomal pathway, with a longer maintenance in the early endosomes and a delayed translocation into the lysosomes. Indeed, internalization of the receptor may not be simply a way to turn off the signal but, on the contrary, the endosomal compartment would play a role as a signalling platform, as it has been observed for other cytokines, such as IL6 and tumour necrosis factor receptor I (Cendrowski et al. 2016; Schmidt-Arras and Rose-John 2021). In support of this hypothesis, experimental evidence show that the weak affinity of the different IL4R sub-

dose response curve an increasing number of EVs was administered to a stable number of cells 5×10^5 cells. Two-way ANOVA with Sidak's multiple comparisons test. (c–d) Kinetic study of BV2 cell response to rIL4 (Red) or EVs *from* Eng IL4 BV2 (Light green) and (e-f) IL4 decorated EVs (Light blue). Real-time PCR for anti-inflammatory marker (c, e) Arg1 and (d, f) Ym1. H3 is used as housekeeping gene. Data are shown as FC ± SEM. Simple linear regression analysis was performed between FC values at the different time points, 0, 1, 3, 6 and 8 h. Ordinary one-way ANOVA, corrected with Tukey's multiple comparisons test was done among the regression lines. (g–h) Kinetic study of BV2 cell response to rIL4 or IL4 EVs enriched isolated from WT and IL4Rα-KO BV2 (Blue-Purple) cell line. Real-time PCR for anti-inflammatory marker (g) Arg1 and (h) Ym1. H3 is used as housekeeping gene. Data are shown as FC ± SEM. Simple linear regression analysis was performed between FC values at the different time points. Ordinary one-way ANOVA, corrected with Tukey's multiple comparisons test was done among the regression lines. Significance is expressed as follows $^*p < 0.05$; $^{**}p < 0.01$; $^{***}p < 0.001$; $^{****}p < 0.0001$.

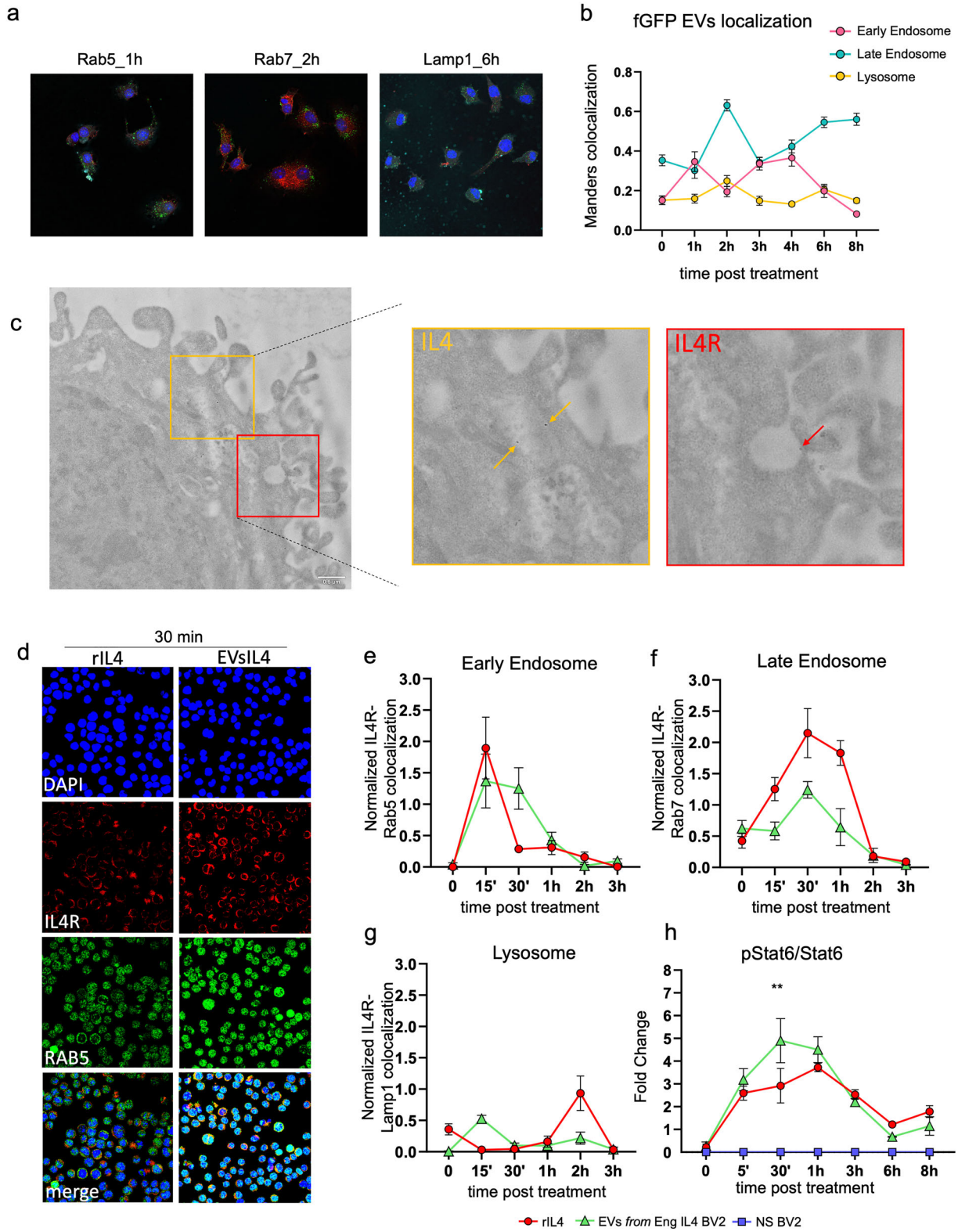

FIGURE 3 | Analysis of IL4R localization across the endosomal pathway after BV2 treatment with either rIL4 or IL4-enriched EVs. (a, b) Immunofluorescence colocalization of fGFP EVs with endosomal pathway markers, Rab5 (early endosomes; Pink), Rab7 (late endosomes; Light blue) and Lamp1 (Lysosomes; Yellow) in BV2 cells at different time points after fGFP EVs treatment (0, 1, 2, 3, 4, 6 and 8 h). (a) Sample images from Leica TCS SP8 SMD FLIM Laser Scanning Confocal (GFP in green 488; IBA1 cyan 633; Rab5, Rab7 and Lamp1 in red 546; Nuclei Dapi). (b) Graph analysis of fGFP fluorescence colocalization showing on y-axis Menders colocalization coefficients. Data are expressed as Mean ± SEM. (c) Transmission Electron Microscopy images of BV2 cells receiving HRP IL4-enriched EVs. Double immunogold staining of IL4Rα (red) and IL4 (yellow) localized in the endosomal pathway. Image from TEM FEI Talos L120C G2 Transmission Electron Microscope. (d–g) Immunofluorescence colocalization of IL4Rα with endosomal pathway markers, Rab5 (early endosomes), Rab7 (late endosomes) and Lamp1 (Lysosomes) in BV2 cells at different time points (0, 15', 30', 1, 2 and 3 h) after rIL4 or EVs *from* Eng IL4 BV2 treatment. (d) Sample images from Leica TCS SP8 SMD FLIM Laser Scanning Confocal (Single

units requires subunit membrane concentration by endocytosis to favour receptor heterodimerization and downstream signalling: in particular, the model proposes that IL4R subunits undergo continuous and constitutive cycles of internalization, regardless ligand stimulation, with a consequent enrichment of signalling endosomes (Gandhi et al. 2014b; Kurgonaite et al. 2015). We believe that the shuttling by EVs might facilitate endosomal signalling of IL4, thanks to the intrinsic EV property to be taken up by recipient cells via endocytosis (Costa Verdera et al. 2017; Mulcahy et al. 2014), a property confirmed in our in vitro system. Whilst our data on P-STAT6 may be indicative of the polarizing capacity of EV-associated IL4 during intracellular signalling, additional studies will be necessary to confirm whether the molecular changes we observed reflect a functional phenotype change. Furthermore, here, we focused exclusively on IL4 due to our previous data showing beneficial effects of this cytokine in vivo (Casella et al. 2018), but available evidence exploring EVs association with different cytokines (Lima et al. 2021; Szabó et al. 2014; Teixeira et al. 2023) is indicative of the complexity of their interaction, pointing to continue their investigation to expand clinical applications.

Our results also show that IL4 is able to efficiently signal in microglial cells not only when packaged inside EVs, but also when decorating them on the outer membrane, which is in line with previous work demonstrating that proteins interacting with the EV surface and hence simply co-isolated with the EVs, can concur to the resulting EV biological effect on receiver cells (Tóth et al. 2021; Wolf et al. 2022). Whilst BV2 cells represent a valid model for basic research, we acknowledge the importance of reproducing the observed results in models that more closely reflect in vivo conditions. Nonetheless, his observation may pave the way for the possibility of engineering microglial EVs upon isolation with the addition of IL4, a procedure with no expected hurdles.

In conclusion, we here show that the association of IL4 with microglia-derived EVs leads to increased anti-inflammatory effect of rIL4 in microglia itself, calling out for further preclinical studies aimed at the design of innovative EV-IL4-based therapeutic strategies to hamper neuroinflammation.

Acknowledgements

This work was supported by FISM Grant 2017/R/12 and by FISM Special Project Hercules. We are grateful to Prof. Marco Biggiogera for the help with TEM.

Conflicts of Interest

The authors declare no conflicts of interest.

Data Availability Statement

The data that support the findings of this study are available on request from the corresponding author. The data are not publicly available due to privacy or ethical restrictions.

References

Agliardi, C., and M. Clerici. 2020. "Blood Extracellular Vesicles (EVs) of central Nervous System Origin: A Window Into the Brain." *Neural Regeneration Research* 15: 55–56. https://doi.org/10.4103/1673-5374.264454.

Alvarez-Erviti, L., Y. Seow, H. Yin, C. Betts, S. Lakhal, and M. J. A. Wood. 2011. "Delivery of siRNA to the Mouse Brain by Systemic Injection of Targeted Exosomes." *Nature Biotechnology* 29: 341–345. https://doi.org/10.1038/nbt.1807.

Bernstein, Z. J., A. Shenoy, A. Chen, N. M. Heller, and J. B. Spangler. 2023. "Engineering the IL-4/IL-13 Axis for Targeted Immune Modulation." *Immunological Reviews* 320: 29–57. https://doi.org/10.1111/imr.13230.

Blasi, E., R. Barluzzi, V. Bocchini, R. Mazzolla, and F. Bistoni. 1990. "Immortalization of Murine Microglial Cells by a v-raf/v-myc Carrying Retrovirus." *Journal of Neuroimmunology* 27: 229–237. https://doi.org/10.1016/0165-5728(90)90073-v.

Butti, E., A. Bergami, A. Recchia, et al. 2008. "IL4 gene Delivery to the CNS Recruits Regulatory T Cells and Induces Clinical Recovery in Mouse Models of Multiple Sclerosis." *Gene Therapy* 15: 504–515. https://doi.org/10.1038/gt.2008.10.

Buzas, E. I. 2023. "The Roles of Extracellular Vesicles in the Immune System." *Nature Reviews Immunology* 23: 236–250. https://doi.org/10.1038/s41577-022-00763-8.

Casella, G., F. Colombo, A. Finardi, et al. 2018. "Extracellular Vesicles Containing IL-4 Modulate Neuroinflammation in a Mouse Model of Multiple Sclerosis." *Molecular Therapy* 26: 2107–2118. https://doi.org/10.1016/j.ymthe.2018.06.024.

Casella, G., L. Garzetti, A. T. Gatta, et al. 2016. "IL4 induces IL6-producing M2 Macrophages Associated to Inhibition of Neuroinflammation In Vitro and In Vivo." *Journal of Neuroinflammation* 13: 139. https://doi.org/10.1186/s12974-016-0596-5.

Cendrowski, J., A. Mamińska, and M. Miaczynska. 2016. "Endocytic Regulation of Cytokine Receptor Signaling." *Cytokine & Growth Factor Reviews* 32: 63–73. https://doi.org/10.1016/j.cytogfr.2016.07.002.

Chen, Z., and B. D. Trapp. 2016. "Microglia and Neuroprotection." *Journal of Neurochemistry* 136: 10–17. https://doi.org/10.1111/jnc.13062.

Costa Verdera, H., J. J. Gitz-Francois, R. M. Schiffelers, and P. Vader. 2017. "Cellular Uptake of Extracellular Vesicles Is Mediated by Clathrin-Independent Endocytosis and Macropinocytosis." *Journal of Controlled Release: Official Journal of the Controlled Release Society* 266: 100–108. https://doi.org/10.1016/j.jconrel.2017.09.019.

Deckers, J., T. Anbergen, A. M. Hokke, et al. 2023. "Engineering Cytokine Therapeutics." *Nature Reviews Bioengineering* 1: 286–303. https://doi.org/10.1038/s44222-023-00030-y.

Delpech, J.-C., S. Herron, M. B. Botros, and T. Ikezu. 2019. "Neuroimmune Crosstalk Through Extracellular Vesicles in Health and Disease." *Trends in Neuroscience (Tins)* 42: 361–372. https://doi.org/10.1016/j.tins.2019.02.007.

Derecki, N. C., A. N. Cardani, C. H. Yang, et al. 2010. "Regulation of Learning and Memory by Meningeal Immunity: A Key Role for IL-4."

channels and merge), 30 min rIL4 or EVs *from* Eng IL4 BV2 (EVs IL4) treatment on BV2 cells (IL4Rα in Red 546; Rab5 in Green 488; Nuclei Dapi). (e–g) Graph analysis of IL4Rα fluorescence colocalization showing on y-axis the IL4Rα signal normalized to the number of positive cells for the endosomal marker (rIL4 treatment in Red and EVs *from* Eng IL4 BV2 treatment in Green). Data are shown as Mean ± SEM. (h) Western blot analysis of Stat6 phosphorylation rate in NS BV2 (Blue) and BV2 treated with rIL4 (Red) or EVs *from* Eng IL4 BV2 (Green), at different time points (0, 5', 30', 1, 3, 6 and 8 h). On y-axis data are shown as ratios between fold change values, normalized on β-actin, of pStat and Stat. Mean ± SEM. Two-way ANOVA with Tukey's multiple comparisons test. Significance is expressed as follows *$p < 0.05$; **$p < 0.01$; ***$p < 0.001$; ****$p < 0.0001$.

Journal of Experimental Medicine 207: 1067–1080. https://doi.org/10.1084/jem.20091419.

DiSabato, D., N. Quan, and J. P. Godbout. 2016. "Neuroinflammation: The Devil Is in the Details." *Journal of Neurochemistry* 139: 136–153. https://doi.org/10.1111/jnc.13607.

Egholm, C., L. E. M. Heeb, D. Impellizzieri, and O. Boyman. 2019. "The Regulatory Effects of Interleukin-4 Receptor Signaling on Neutrophils in Type 2 Immune Responses." *Frontiers in immunology* 10: 2507. https://doi.org/10.3389/fimmu.2019.02507.

Erickson, M. A., and W. A. Banks. 2018. "Neuroimmune Axes of the Blood–Brain Barriers and Blood–Brain Interfaces: Bases for Physiological Regulation, Disease States, and Pharmacological Interventions." *Pharmacological Reviews* 70: 278–314. https://doi.org/10.1124/pr.117.014647.

Furlan, R., P. L. Poliani, F. Galbiati, et al. 1998. "Central Nervous System Delivery of Interleukin 4 by a Nonreplicative Herpes Simplex Type 1 Viral Vector Ameliorates Autoimmune Demyelination." *Human Gene Therapy* 9: 2605–2617. https://doi.org/10.1089/hum.1998.9.17-2605.

Furlan, R., P. L. Poliani, P. C. Marconi, et al. 2001. "Central Nervous System Gene Therapy With Interleukin-4 Inhibits Progression of Ongoing Relapsing–Remitting Autoimmune Encephalomyelitis in Biozzi AB/H Mice." *Gene Therapy* 8: 13–19. https://doi.org/10.1038/sj.gt.3301357.

Gabrielli, M., S. Raffaele, M. Fumagalli, and C. Verderio. 2022. "The Multiple Faces of Extracellular Vesicles Released by Microglia: Where Are We 10 Years After?" *Frontiers in Cellular Neuroscience* 16: 984690. https://doi.org/10.3389/fncel.2022.984690.

Gadani, S. P., J. C. Cronk, G. T. Norris, and J. Kipnis. 2012. "Interleukin-4: A Cytokine to Remember." *Journal of Immunology Baltim Md 1950* 189: 4213–4219. https://doi.org/10.4049/jimmunol.1202246.

Gandhi, H., R. Worch, K. Kurgonaite, et al. 2014a. "Dynamics and Interaction of Interleukin-4 Receptor Subunits in Living Cells." *Biophysical Journal* 107: 2515–2527. https://doi.org/10.1016/j.bpj.2014.07.077.

Gandhi, H., R. Worch, K. Kurgonaite, et al. 2014b. "Dynamics and Interaction of Interleukin-4 Receptor Subunits in Living Cells." *Biophysical Journal* 107: 2515–2527. https://doi.org/10.1016/j.bpj.2014.07.077.

Gao, C., J. Jiang, Y. Tan, and S. Chen. 2023. "Microglia in Neurodegenerative Diseases: Mechanism and Potential Therapeutic Targets." *Signal Transduction and Targeted Therapy* 8: 359. https://doi.org/10.1038/s41392-023-01588-0.

Gärtner, Y., L. Bitar, F. Zipp, and C. F. Vogelaar. 2023. "Interleukin-4 as a Therapeutic Target." *Pharmacology & Therapeutics* 242: 108348. https://doi.org/10.1016/j.pharmthera.2023.108348.

Guedes, J. R., P. A. Ferreira, J. Costa, et al. 2023. "IL-4 Shapes Microglia-Dependent Pruning of the Cerebellum During Postnatal Development." *Neuron* 111: 3435–3449.e8. https://doi.org/10.1016/j.neuron.2023.09.031.

He, Y., Y. Gao, Q. Zhang, G. Zhou, F. Cao, and S. Yao. 2020. "IL-4 Switches Microglia/Macrophage M1/M2 Polarization and Alleviates Neurological Damage by Modulating the JAK1/STAT6 Pathway Following ICH." *Neuroscience* 437: 161–171. https://doi.org/10.1016/j.neuroscience.2020.03.008.

Hermann, D. M., L. Peruzzotti-Jametti, B. Giebel, and S. Pluchino. 2023. "Extracellular Vesicles Set the Stage for Brain Plasticity and Recovery by Multimodal Signalling." *Brain* 147: 372–389. https://doi.org/10.1093/brain/awad332.

Jeppesen, D. K., A. M. Fenix, J. L. Franklin, et al. 2019. "Reassessment of Exosome Composition." *Cell* 177: 428–445.e18. https://doi.org/10.1016/j.cell.2019.02.029.

Jiang, X., S. Yi, Q. Liu, and J. Zhang. 2022. "The Secretome of Microglia Induced by IL-4 of IFN-γ Differently Regulate Proliferation, Differentiation and Survival of Adult Neural Stem/Progenitor Cell by Targeting the PI3K-Akt Pathway." *Cytotechnology* 74: 407–420. https://doi.org/10.1007/s10616-022-00534-2.

Junttila, I. S. 2018. "Tuning the Cytokine Responses: An Update on Interleukin (IL)-4 and IL-13 Receptor Complexes." *Frontiers in immunology* 9: 888. https://doi.org/10.3389/fimmu.2018.00888.

Kanada, M., M. H. Bachmann, J. W. Hardy, et al. 2015. "Differential Fates of Biomolecules Delivered to Target Cells via Extracellular Vesicles." *Proceedings of the National Academy of Sciences of the United States of America* 112: E1433–E1442. https://doi.org/10.1073/pnas.1418401112.

Krämer-Albers, E.-M. 2022. "Extracellular Vesicles at CNS Barriers: Mode of Action." *Current Opinion in Neurobiology* 75: 102569. https://doi.org/10.1016/j.conb.2022.102569.

Kurgonaite, K., H. Gandhi, T. Kurth, et al. 2015. "Essential Role of Endocytosis for Interleukin-4 Receptor Mediated JAK/STAT Signalling." *Journal of Cell Science* 128, no. 20: 3781–3795. https://doi.org/10.1242/jcs.170969.

Li, Q., and B. A. Barres. 2018. "Microglia and Macrophages in Brain Homeostasis and Disease." *Nature Reviews Immunology* 18: 225–242. https://doi.org/10.1038/nri.2017.125.

Lima, L. G., S. Ham, H. Shin, et al. 2021. "Tumor Microenvironmental Cytokines Bound to Cancer Exosomes Determine Uptake by Cytokine Receptor-Expressing Cells and Biodistribution." *Nature Communications* 12: 3543. https://doi.org/10.1038/s41467-021-23946-8.

Lizarraga-Valderrama, L. R., and G. K. Sheridan. 2021. "Extracellular Vesicles and Intercellular Communication in the Central Nervous System." *Journal of the Federation of European Biochemical Societies* 595: 1391–1410. https://doi.org/10.1002/1873-3468.14074.

Mulcahy, L. A., R. C. Pink, and D. R. F. Carter. 2014. "Routes and Mechanisms of Extracellular Vesicle Uptake." *Journal of Extracellular Vesicles* 3: 24641. https://doi.org/10.3402/jev.v3.24641.

Mustapic, M., E. Eitan, J. K. Werner, et al. 2017. "Plasma Extracellular Vesicles Enriched for Neuronal Origin: A Potential Window Into Brain Pathologic Processes." *Frontiers in Neuroscience* 11: 278. https://doi.org/10.3389/fnins.2017.00278.

Orihuela, R., C. A. McPherson, and G. J. Harry. 2016. "Microglial M1/M2 Polarization and Metabolic States." *British Journal of Pharmacology* 173: 649–665. https://doi.org/10.1111/bph.13139.

Poliani, P. L., H. Brok, R. Furlan, et al. 2001. "Delivery to the Central Nervous System of a Nonreplicative Herpes Simplex Type 1 Vector Engineered With the Interleukin 4 Gene Protects Rhesus Monkeys From Hyperacute Autoimmune Encephalomyelitis." *Human Gene Therapy* 12: 905–920. https://doi.org/10.1089/104303401750195872.

Prinz, M., S. Jung, and J. Priller. 2019. "Microglia Biology: One Century of Evolving Concepts." *Cell* 179: 292–311. https://doi.org/10.1016/j.cell.2019.08.053.

Quarta, A., Z. Berneman, and P. Ponsaerts. 2020. "Neuroprotective Modulation of Microglia Effector Functions Following Priming With Interleukin 4 and 13: Current Limitations in Understanding Their Mode-of-action." *Brain, Behavior, and Immunity* 88: 856–866. https://doi.org/10.1016/j.bbi.2020.03.023.

Ransohoff, R. M. 2016. "How Neuroinflammation Contributes to Neurodegeneration." *Science* 353: 777–783. https://doi.org/10.1126/science.aag2590.

Saint-Pol, J., F. Gosselet, S. Duban-Deweer, G. Pottiez, and Y. Karamanos. 2020. "Targeting and Crossing the Blood-Brain Barrier With Extracellular Vesicles." *Cells* 9: 851. https://doi.org/10.3390/cells9040851.

Saxton, R. A., C. R. Glassman, and K. C. Garcia. 2023. "Emerging Principles of Cytokine Pharmacology and Therapeutics." *Nature Reviews Drug Discovery* 22: 21–37. https://doi.org/10.1038/s41573-022-00557-6.

Schmidt-Arras, D., and S. Rose-John. 2021. "Endosomes as Signaling Platforms for IL-6 Family Cytokine Receptors." *Frontiers in Cell and Developmental Biology* 9: 688314. https://doi.org/10.3389/fcell.2021.688314.

Szabó, G. T., B. Tarr, K. Pálóczi, et al. 2014. "Critical Role of Extracellular Vesicles in Modulating the Cellular Effects of Cytokines." *Cellular and molecular life sciences CMLS* 71: 4055–4067. https://doi.org/10.1007/s00018-014-1618-z.

Teixeira, A. F., Y. Wang, J. Iaria, P. ten Dijke, and H.-J. Zhu. 2023. "Simultaneously Targeting Extracellular Vesicle Trafficking and TGF-β Receptor Kinase Activity Blocks Signaling Hyperactivation and Metastasis." *Signal Transduction and Targeted Therapy* 8: 456. https://doi.org/10.1038/s41392-023-01711-1.

Tóth, E. Á., L. Turiák, T. Visnovitz, et al. 2021. "Formation of a Protein Corona on the Surface of Extracellular Vesicles in Blood Plasma." *Journal of Extracellular Vesicles* 10: e12140. https://doi.org/10.1002/jev2.12140.

Verderio, C., L. Muzio, E. Turola, et al. 2012. "Myeloid Microvesicles Are a Marker and Therapeutic Target for Neuroinflammation." *Annals of Neurology* 72: 610–624. https://doi.org/10.1002/ana.23627.

Vogelaar, C. F., S. Mandal, S. Lerch, et al. 2018. "Fast Direct Neuronal Signaling via the IL-4 Receptor as Therapeutic Target in Neuroinflammation." *Science Translational Medicine* 10: eaao2304. https://doi.org/10.1126/scitranslmed.aao2304.

Wang, J., L. Wang, Q. Wu, et al. 2024. "Interleukin-4 Modulates Neuroinflammation by Inducing Phenotypic Transformation of Microglia Following Subarachnoid Hemorrhage." *Inflammation* 47: 390–403. https://doi.org/10.1007/s10753-023-01917-z.

Welsh, J. A., D. C. I. Goberdhan, L. O'Driscoll, et al. 2024. "Minimal Information for Studies of Extracellular Vesicles (MISEV2023): From Basic to Advanced Approaches." *Journal of Extracellular Vesicles* 13: e12404. https://doi.org/10.1002/jev2.12404.

Wiklander, O. P. B., M. Á. Brennan, J. Lötvall, X. O. Breakefield, and S. E. Andaloussi. 2019. "Advances in Therapeutic Applications of Extracellular Vesicles." *Science Translational Medicine* 11: eaav8521. https://doi.org/10.1126/scitranslmed.aav8521.

Wolf, M., R. W. Poupardin, P. Ebner-Peking, et al. 2022. "A Functional Corona Around Extracellular Vesicles Enhances Angiogenesis, Skin Regeneration and Immunomodulation." *Journal of Extracellular Vesicles* 11: e12207. https://doi.org/10.1002/jev2.12207.

Yáñez-Mó, M., P. R.-M. Siljander, Z. Andreu, et al. 2015. "Biological Properties of Extracellular Vesicles and Their Physiological Functions." Journal of Extracellular Vesicles 4. https://doi.org/10.3402/jev.v4.27066.

Yong, V. W. 2022. "Microglia in Multiple Sclerosis: Protectors Turn Destroyers." *Neuron* 110: 3534–3548. https://doi.org/10.1016/j.neuron.2022.06.023.

Zhang, W., D. Xiao, Q. Mao, and H. Xia. 2023. "Role of Neuroinflammation in Neurodegeneration Development." *Signal Transduction and Targeted Therapy* 8: 267. https://doi.org/10.1038/s41392-023-01486-5.

Supporting Information

Additional supporting information can be found online in the Supporting Information section.

Supplementary Figures: jex270111-sup-0001-Figures.docx **Supplementary Tables**: jex270111-sup-0002-Tables.docx